Anisotropic Bremsstrahlung Emission and the form of Regularized Electron Flux Spectra in Solar Flares

Anna Maria Massone[1], A. Gordon Emslie[2], Eduard P. Kontar[4],
Michele Piana[1,3], Marco Prato[1,3], & John C. Brown[4]

ABSTRACT

The cross-section for bremsstrahlung photon emission in solar flares is in general a function of the angle θ between the incoming electron and the outgoing photon directions. Thus the electron spectrum required to produce a given photon spectrum is a function of this angle, which is related to the position of the flare on the solar disk and the direction(s) of the pre-collision electrons relative to the local solar vertical. We compare mean electron flux spectra for the flare of August 21, 2002, using cross-sections for parameterized ranges of the angle θ. Implications for the shape of the mean source electron spectrum, and for the injected power in nonthermal electrons, are discussed.

Subject headings: Sun: flares, Sun: X-rays

1. Introduction

Piana et al. (2003) have shown how to apply a regularized inversion technique to high-resolution hard X-ray spectra from solar flares in order to recover knowledge about the electron flux spectrum in the source. In their analysis they used a solid-angle-averaged form (Haug 1997) for the bremsstrahlung cross-section $Q(\epsilon, E)$. However, the actual cross-section $Q(\epsilon, E)$ is in general a function not only of the photon energy ϵ and electron energy E, but also of the incoming and outgoing electron directions and of the polarization state of the

[1]INFM, UdR di Genova, via Dodecaneso 33, I-16146 Genova, Italy
massone@ge.infm.it, piana@dima.unige.it, prato@dima.unige.it

[2]Department of Physics, The University of Alabama in Huntsville,Huntsville, AL 35899
emslieg@email.uah.edu

[3]Dipartimento di Matematica, Università di Genova, via Dodecaneso 35, I-16146 Genova, Italy

[4]Department of Physics & Astronomy, The University, Glasgow G12 8QQ, UK
eduard@astro.gla.ac.uk, john@astro.gla.ac.uk

emitted photon (Gluckstern, Hull, & Breit 1953). It is also composed of components due to both electron-ion and electron-electron bremsstrahlung, although it can be shown that the latter is quite negligible except at mildly or extremely relativistic energies. Gluckstern & Hull (1953) have presented expressions for the electron-proton bremsstrahlung cross-section, integrated over the direction of the outgoing electron and summed over the polarization states of the emitted photon. The resulting cross-section $Q(\epsilon, E; \theta)$, differential in energy and solid angle of the incoming electron direction, is a function of three variables: the photon energy ϵ (keV), the electron energy E (keV), and θ, the angle between the pre-collision electron velocity vector and the direction of photon emission. Various authors (e.g., Elwert & Haug 1970, 1971; Brown 1972; Haug 1972; Hénoux 1975; Langer & Petrosian 1977; Leach & Petrosian 1983) have shown how the hard X-ray emission from a prescribed electron source function varies with viewing direction.

The variation of $Q(\epsilon, E; \theta)$ with θ can be very significant, particularly at moderate or large ($\gtrsim$30 keV) electron and photon energies. Furthermore, the variation of $Q(\epsilon, E; \theta)$ with E is significantly different for different θ. For example, for a fixed photon energy ϵ and $\theta \lesssim 30°$, the cross-section increases monotonically with E. However, for a fixed ϵ and $\theta \gtrsim 30°$, the cross-section initially increases with E but then reaches a maximum and subsequently decreases with E, roughly like E^{-1} (the angle-averaged cross-section has a very similar behavior). Hence the relation between the electron and photon spectra depends critically on using the correct value (or range of values) for the emission angle θ. For example, in the July 23, 2002 event analyzed by Piana et al. (2003), the flare is located at a heliocentric angle $\sim 70°$; a vertically downward electron beam therefore corresponds to a viewing angle $\theta \sim 110°$, for which the cross-section $Q(\epsilon, E; \theta)$ differs significantly from the solid-angle-averaged value which they, and others, have used.

The correct cross-section to use must in practice take into account two important aspects of the geometrical and physical environment. First, there will in general be a significant spread in the incoming directions of the electrons, due to spiralling around magnetic field lines, magnetic mirroring in non-uniform field geometries and directional modification due to Coulomb collisions and collective (wave-particle) processes (e.g., Kontar 2001; Kontar and Pecseli 2002). Second, Smith et al. (2003) have shown that the observed redshifts in prompt gamma-ray line profiles suggest that the guiding magnetic field may be inclined away from the vertical toward the observer, and a similar inclination in guiding field direction angle may be appropriate for the bremsstrahlung-producing electron beam (although it should be noted that the electron and ion accelerations may well operate on fundamentally different bundles of magnetic field – Hurford et al. 2003; Emslie, Miller, & Brown 2004).

Let us now generalize the concept of the mean source electron flux spectrum (Brown

1971; Brown, Emslie, & Kontar 2003) to the case of an anisotropic cross-section and/or source electron distribution function. The hard X-ray intensity $I(\epsilon)$ observed at distance R from a source can be written as

$$I(\epsilon) = \frac{1}{4\pi R^2} \int_{E=\epsilon}^{\infty} \int_{\Omega} \int_{V} Q(\epsilon, E; \theta)\, F(E, \mathbf{r}, \Omega)\, n(\mathbf{r})\, dV\, d\Omega\, dE, \tag{1}$$

where $F(E, \mathbf{r}, \Omega)$ is the electron flux differential in electron kinetic energy E, position $\mathbf{r}$ and solid angle of the incoming electron direction Ω, and $Q(\epsilon, E; \theta)$ is the cross-section for bremsstrahlung emission in the direction of the observer. If we define

$$\hat{F}(E, \Omega) = \frac{\int F(E, \mathbf{r}, \Omega)\, n(\mathbf{r})\, dV}{\int n(\mathbf{r})\, dV} = \frac{\int F(E, \mathbf{r}, \Omega)\, n(\mathbf{r})\, dV}{\bar{n} V}, \tag{2}$$

where $\bar{n} = (1/V) \int n(\mathbf{r})\, dV$, then Equation (1) may be written as

$$I(\epsilon) = \frac{\bar{n} V}{4\pi R^2} \int_{E=\epsilon}^{\infty} \int_{\Omega} Q(\epsilon, E; \theta)\, \hat{F}(E, \Omega)\, d\Omega\, dE. \tag{3}$$

If $\hat{F}(E, \Omega)$ is isotropic, then we define $\overline{F}(E) \equiv \hat{F}(E)$ and let

$$\overline{Q}(\epsilon, E) = \int_{\Omega} Q(\epsilon, E; \theta)\, d\Omega. \tag{4}$$

Then we can write

$$I(\epsilon) = \frac{\bar{n} V}{4\pi R^2} \int_{E=\epsilon}^{\infty} \overline{F}(E)\, \overline{Q}(\epsilon, E)\, dE. \tag{5}$$

This is the expression used by Brown, Emslie, & Kontar (2003) to define the *mean source electron spectrum* $\overline{F}(E)$. It should be noted that Equation (5) also applies in the (somewhat hypothetical) case where $Q(\epsilon, E; \theta)$ is independent of θ, with $\overline{Q} \equiv Q$ and

$$\overline{F}(E) = \int_{\Omega} \hat{F}(E, \Omega)\, d\Omega. \tag{6}$$

In the physically realistic case, however, neither $Q(\epsilon, E; \theta)$ nor $\hat{F}(E, \Omega)$ is isotropic and Equation (3) cannot be uniquely inverted to obtain $\hat{F}(E, \Omega)$ from observations of $I(\epsilon)$. To do this we would need bivariate stereo data on $dI(\epsilon, \Omega)/d\Omega$. To make progress, therefore, requires some further assumptions on the form of $\hat{F}(E, \Omega)$. In this paper we restrict ourselves to the simplest assumption, namely that $\hat{F}(E, \Omega)$ is separable in E and Ω, i.e.,

$$\hat{F}(E,\Omega) = \overline{F}(E)\,\frac{h(\Omega)}{\int_\Omega h(\Omega)\,d\Omega}. \tag{7}$$

With such an assumption, Equation (3) may be written

$$I(\epsilon) = \frac{\bar{n}V}{4\pi R^2}\int_{E=\epsilon}^{\infty}\overline{F}(E)\,dE\left[\frac{\int_\Omega Q(\epsilon,E;\theta)\,h(\Omega)\,d\Omega}{\int_\Omega h(\Omega)\,d\Omega}\right]. \tag{8}$$

If we then define

$$\overline{Q}(\epsilon,E) = \frac{\int_\Omega Q(\epsilon,E;\theta)\,h(\Omega)\,d\Omega}{\int_\Omega h(\Omega)\,d\Omega}, \tag{9}$$

then Equation (8) is formally identical to Equation (5) and can be solved for any adopted form of $h(\Omega)$ once $\overline{Q}(\epsilon,E)$ is evaluated using Equation (9). Note that in practice – e.g., in a collisional thick target – the E and Ω dependencies of $\hat{F}(E,\Omega)$ are *not* separable and further vary along the electron paths. To deal with that situation more properly requires explicit modeling of the electron propagation - i.e., of electron scattering and energy losses; in general this can probably only be done by forward modeling. Nevertheless, the results of our separable inversion formulation will provide a better starting point than the assumption of isotropy used hitherto.

In §2 we review the form of the bremsstrahlung cross-section and in §3 we present the data to be used for the analysis. In §4 we present results for incoming electrons traveling both in a single direction and over a range of directions; these results are discussed in §5. In §6 we present our conclusions.

2. Form of the Cross-Section

The form of the angle-dependent electron-ion bremsstrahlung cross-section $Q(\epsilon,E;\theta)$ has been given by Gluckstern & Hull (1953) and Koch & Motz (1959; formula 2BN) and is reproduced in Appendix A. (Forms of the cross-section for each polarization state have also been given by Bai & Ramaty [1978]. These expressions correct a typographical error in Gluckstern & Hull [1953] which does not, however, appear in the expression for the polarization-summed cross-section.) Expressions for the solid-angle-averaged cross-section $Q(\epsilon,E)$ have also been given by Koch & Motz (1959; formula 3BN); this cross-section is here denoted by $Q_{4\pi}$. We verified the correct normalization ($\frac{1}{4\pi}\int Q(\epsilon,E;\theta)\sin\theta\,d\theta\,d\phi = Q_{4\pi}$) through numerical integration for a variety of values of ϵ and E.

As is shown in the Appendix (see Figure 7), for electron energies $E \gg \epsilon$, the form of $q(\epsilon, E; \theta)$ is a decreasing function of θ: there is a preference for photons to be emitted in the direction of the incoming electron. However, at electron energies comparable to the photon energy there must of necessity be a substantial scattering angle between the incoming and outgoing electrons, and hence the photons tend to be emitted preferentially at a significant angle relative to the incoming electron velocity. Hence, at electron energies $E \gtrsim \epsilon$, the cross-section peaks not in the forward direction but rather at a modest angle $(30 - 40)^\circ$ (see Figure 7).

3. Data

We selected the event of August 21, 2002 (00:39:04-00:39:48 UT) for our analysis. This event selection was based on two factors. First, in an effort to reduce the complexity of the problem, we sought to analyze individual impulsive "spikes" within an event, on the grounds that it is more likely that each such time interval corresponds to a single injection event, with a corresponding single geometry throughout the burst. For the August 21 event there was indeed a clear identification of impulsive "spikes" in the flare light curve. Second, the count rates in that event were sufficiently low that pulse pileup in the RHESSI detectors (Smith et al. 2002) was not a significant factor. (The somewhat mysterious "dip" in the $\overline{F}(E)$ spectrum obtained by Piana et al. [2003] for the July 23, 2002 [$\sim$ 0030 UT] event occurs at an energy that is particularly susceptible to pulse pileup issues in very large events; the effect of pulse pileup on the conversion from count to photon spectra is not yet completely understood.)

The location of the flare on the solar disk is $x = 696'', y = -248''$, which corresponds to a heliocentric angle of $\sim 50^\circ$. Figure 1 shows the light curves at different photon energies and the choice of time interval (00:39:04-00:39:48 UT) for subsequent analysis; Figure 2 shows the photon spectrum for that time interval. This spectrum was obtained by processing the RHESSI count spectrum through the SPEX software on the Solar Software tree, and is robust in the count/photon energy range considered.

4. Determination of $\overline{F}(E)$ as a Function of Viewing Angle

Piana et al. (2003) and Kontar et al. (2004) have discussed how Equation (5) can be solved for an optimal reconstruction of $\overline{F}(E)$ for a given observed spectrum $I(\epsilon)$ and cross-section $\overline{Q}(\epsilon, E)$; it should be noted that the Equation (5) is of Volterra (rather than

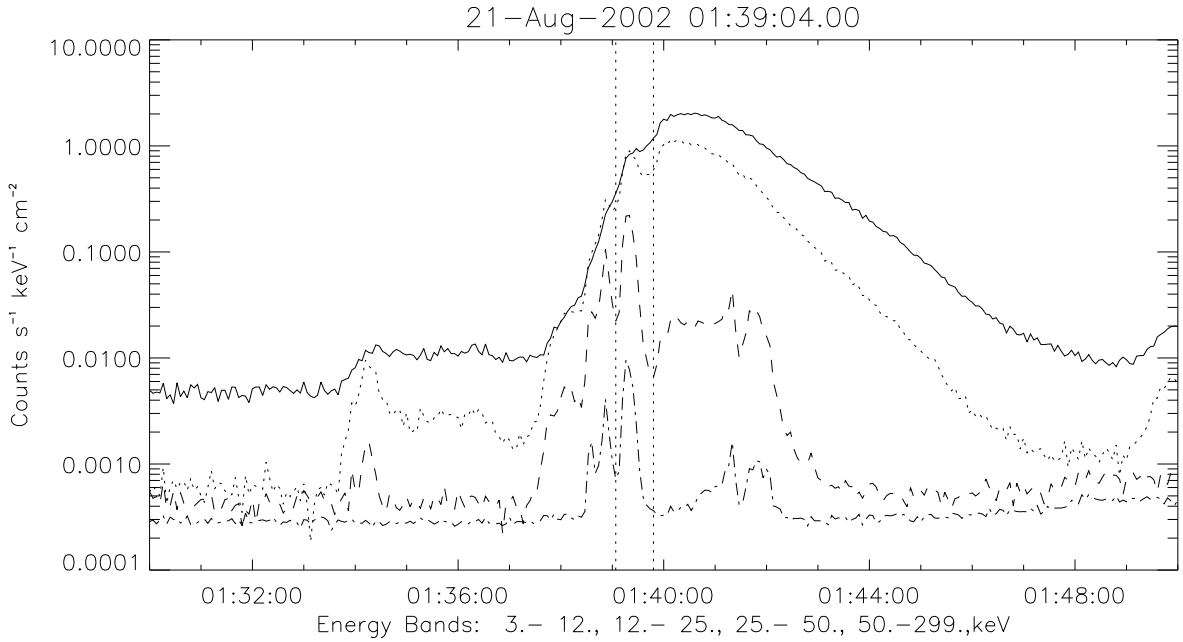

Fig. 1.— Light curves for the August 21, 2002 event. The two vertical dashed lines show the time interval (01:39:04 - 01:39:48 UT) selected for analysis. The energy bands shown are 3–12 keV (solid), 12–25 keV (dotted), 25–50 keV (dashed) and 50–299 keV (dot-dashed).

Fredholm) form and hence has a degree of ill-posedness that is small enough for manageable error control in the recovered $\overline{F}(E)$ solution. The form of $\overline{F}(E)$ can be used to establish a wide variety of physically significant features of the flare, such as the differential emission measure $\xi(T)$ under a thermal interpretation of the electron distribution, or the injected electron flux under a non-thermal thick-target interpretation (Brown & Emslie 1988). It is therefore important to determine the extent to which these physically significant functions depend on the viewing angle θ.

It is important to realize that electrons in general have a finite pitch angle to the guiding magnetic field lines about which they spiral, so that the incoming electrons have a wide range of directions. The details of the electron pitch angle distribution depend on a number of physical effects. Collisions with ambient electrons and protons broaden the angular distribution about the original injected direction, with the mean pitch angle (Brown 1972) and breadth (Leach & Petrosian 1981) of the distribution increasing with depth in the target. Interaction with plasma waves, notably whistlers (e.g., Stepanov & Tsap 2002) may rapidly isotropize an electron beam and create a "fan" distribution with significant momentum perpendicular to the guiding magnetic field.

As discussed in the Introduction, a complete investigation of the form of the pitch angle distribution of the incoming electrons is beyond the scope of this paper. We therefore make the assumption that at all energies the target-averaged incoming electron velocities are uniformly distributed over solid angle within a cone of half-angle α centered on a direction that makes an angle θ_0 relative to the direction of photon emission, i.e. (with β as the polar angle relative to the axis of the cone)

$$h(\Omega) = \begin{cases} 1 & \beta \leq \alpha \\ 0 & \text{otherwise.} \end{cases} \tag{10}$$

With this form of $h(\Omega)$ the average cross-section $\overline{Q}(\epsilon, E)$ (Equation [9]) is

$$\overline{Q}(\epsilon, E; \theta_0, \alpha) = \frac{1}{2\pi(1-\cos\alpha)} \int_{\phi=0}^{2\pi} \int_{\beta=0}^{\alpha} Q(\epsilon, E; \theta) \sin\beta \, d\beta \, d\phi, \tag{11}$$

where θ is the angle between the observer and an elementary electron beam oriented at polar coordinates (β, ϕ) relative to the axis of the cone, viz.

$$\cos\theta = \cos\theta_0 \, \cos\beta + \sin\theta_0 \, \sin\beta \, \cos\phi. \tag{12}$$

We then perform the inversion of Equation (5) using the appropriate form of $\overline{Q}(\epsilon, E; \theta_0, \alpha)$ with $Z^2 = 1.44$. The photon spectral data $I(\epsilon)$ were taken over the range 9-222 keV (be-

low 9 keV there is a substantial contribution to the observed spectrum from line emission not dealt with with the free-free cross-section $Q[\epsilon, E]$, and above the upper limit data noise and background subtraction made some inferred photon rates negative). We constructed regularized forms of $\overline{F}_{\theta_0,\alpha}(E)$ for mean angles θ_0 over the range from 0° (photon emission parallel to the direction of the incoming electron) to 180° (photon emission in the antiparallel direction). For vertically-downward directed electron beams, values of $\theta_0 \sim 180°$ are appropriate for disk-center events, and values $\theta_0 \sim 90°$ are appropriate for events near the limb. A variety of α values ($10°, 30°, 60°, 90°$ and 180°) were used; we found that the results for values of $\alpha < 10°$ were indistinguishable from the results for $\alpha = 10°$. Note also that the last of these ($\alpha = 180°$) corresponds to an integration over the entire sphere, i.e., to the angle-averaged cross-section $Q_{4\pi}$. A "confidence strip" of $\overline{F}_{\theta_0,\alpha}(E)$ forms based on different realizations of the (noisy) data was produced for each photon spectrum $I(\epsilon)$ and the mean of this confidence strip was used for further analysis.

The August 21 flare was located at a heliocentric angle of approximately 50°. If we assume that the mean direction of the incoming electrons was vertically downward at this location, then the corresponding value of θ_0 is 130°. Figure 3 shows the reconstructed $\overline{F}_{\theta_0,\alpha}(E)$ corresponding to $\theta_0 = 130°$ and various values of α, including $\alpha = 180°$, corresponding to the solid-angle-averaged cross-section.

It should be recognized that the assumption of a vertical mean incoming electron direction, and so the choice of $\theta_0 = 130°$ is not rigorously justified. For comparison, therefore, Figure 4 shows the same results for values of θ_0 ranging from 0° to 180° in 45° steps.

5. Discussion

We begin by discussing the forms of $\overline{F}_{\theta_0,\alpha}(E)$ for a prescribed θ_0, namely the nominal 130° value of Figure 3, corresponding to a cone of electrons with a vertically downward axis of symmetry.

A value $\alpha = 0$ corresponds to all the emission concentrated at $\theta = \theta_0$. However, for nonzero α, we now have emission spread over a range of θ from $\theta_o - \alpha$ to $\theta_o + \alpha$. Because of the asymmetric form of the emission polar diagram at high electron energies (Figure 7), the enhanced emission in the $\theta_o - \alpha$ direction more than compensates for the decrease emission in the $\theta_o + \alpha$ direction, so that fewer total electrons are required to produce a given photon flux than for the unidirectional ($\alpha = 0$) case. Figure 3 shows that the magnitude of the reconstructed $\overline{F}_{\theta_0,\alpha}(E)$ does indeed depend quite strongly on the range of incoming electron directions α, especially at high electron energies E (at 500 keV, the required electron flux

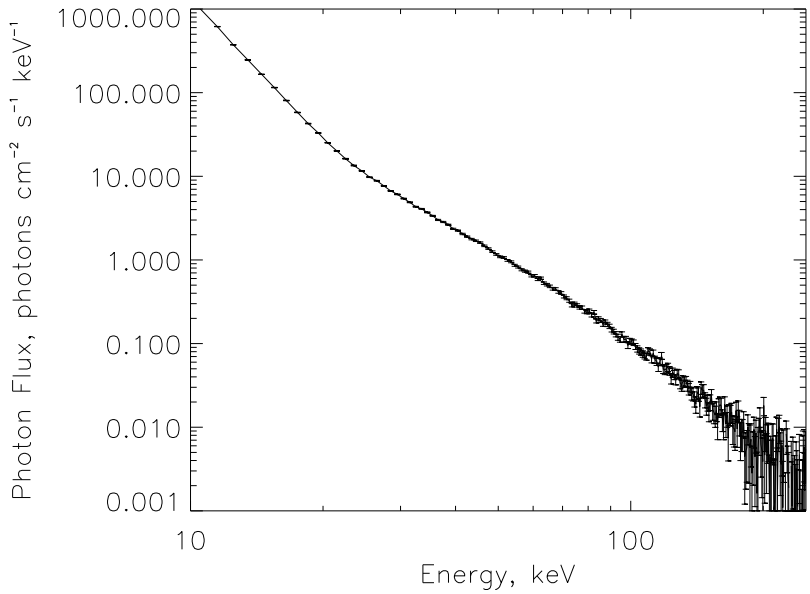

Fig. 2.— Photon spectra for the time interval (01:39:04 – 01:39:48 UT) indicated in Figure 1.

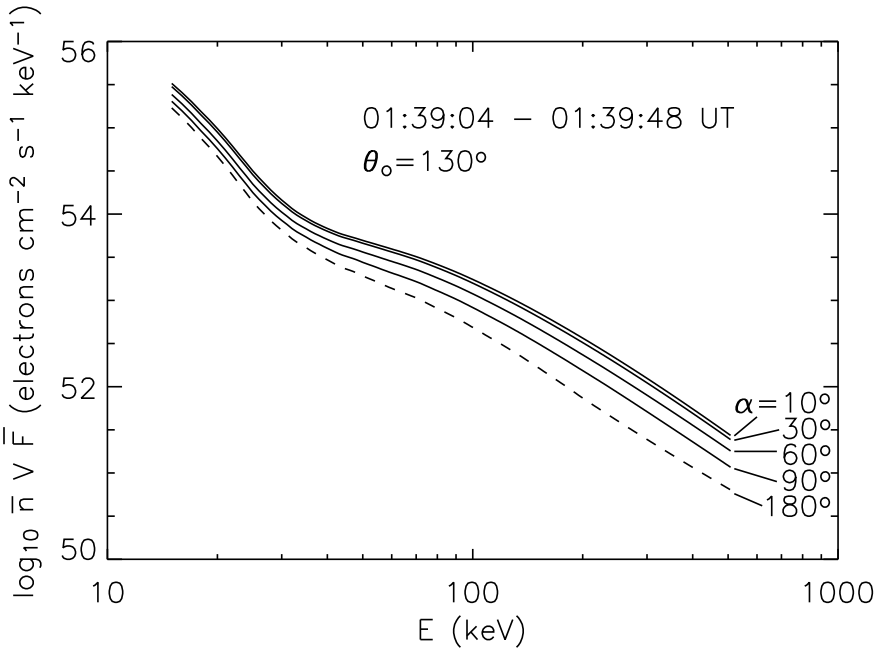

Fig. 3.— $\overline{F}_{\theta_0,\alpha}(E)$ for $\theta_0 = 130°$ and the values of α (spread in incoming electron directions) shown. The dashed curve (labeled $\alpha = 180°$) is the spectrum obtained using the angle-averaged cross-section $Q_{4\pi}$.

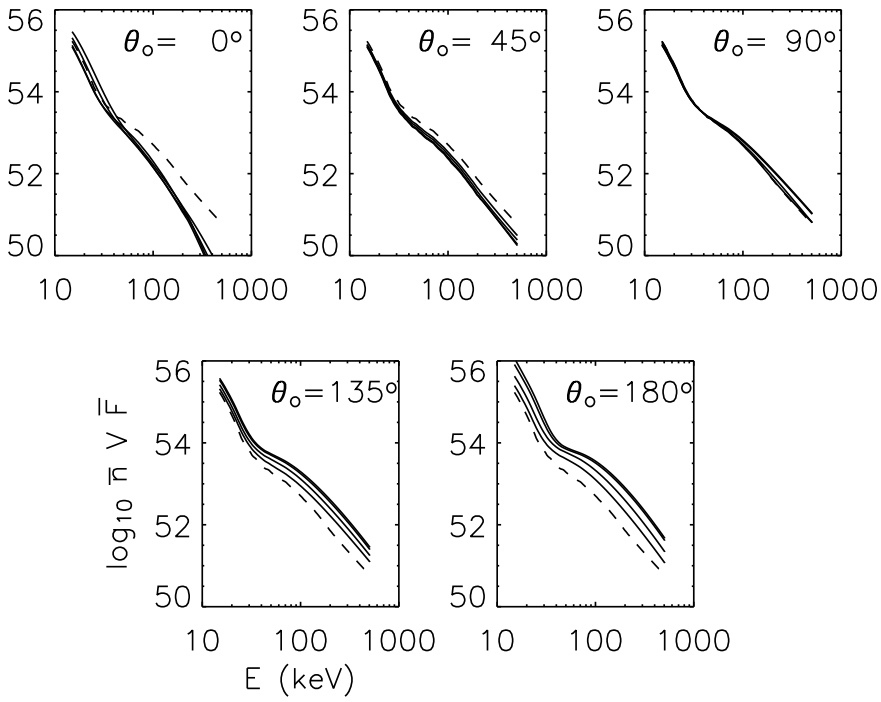

Fig. 4.— As for Figure 3, but for values of $\theta_0 = 0°, 45°, 90°, 135°$ and 180°. The curves have the same significance as in Figure 3, with the uppermost solid curves corresponding to the lowest values of α.

is less by a factor of ~ 4). Since this effect becomes more important with increasing energy (Figure 3), the reconstructed $\overline{F}_{\theta_0,\alpha}(E)$ also becomes *steeper* with increasing α. Recognizing that the extreme maximum case $\alpha = 180^\circ$ corresponds to the angle-averaged cross-section used in previous papers (e.g., Piana et al. 2003), we see that the use of a cross-section that more realistically reflects the range of incoming electron velocity vectors always *flattens* the high-energy part of the inferred electron spectrum relative to that found using the angle-averaged cross-section $Q_{4\pi}$. For values of $\alpha \lesssim 10^\circ$, the effect "saturates," i.e., there is little to distinguish between values of α in the range $0 \leq \alpha \leq 10^\circ$.

Next we discuss the variation of $\overline{F}_{\theta_0,\alpha}(E)$ with mean viewing angle θ_0. For $\theta_0 = 180^\circ$ (Figure 4), corresponding to vertically-downward electrons in a disk center flare, the recovered flux $\overline{F}_{\theta_0,\alpha}(E)$ for modest values of α is, at high energies, significantly (an order of magnitude or so) greater than the value of $\overline{F}_{\theta_0,180^\circ}(E)$, i.e., to use of the angle-averaged cross-section $Q_{4\pi}$. This is because of the very low values of the normalized cross-section $q(\epsilon, E; \theta)$ appropriate to this viewing angle (Figure 7), and hence the inefficiency of photon production in such a direction. Such large fluxes may introduce issues of beam stability. Conversely, for $\theta_0 = 90^\circ$ (corresponding to vertically-downward electrons in a limb flare; see Figure 4), the enhancement over the angle-averaged ($\alpha = 180^\circ$) case is less pronounced; indeed the recovered spectra are remarkably similar to that derived using the angle-averaged cross-section, particularly at energies $\gtrsim 30$ keV.

Values of $\theta_0 < 90^\circ$ correspond to the case where the mean velocity of the electrons has a component *toward* the observer, and therefore *away* from the Sun. In general, θ_0 values in this first quadrant lead (Figure 4) to a *decreased* value of $\overline{F}_{\theta_0,\alpha}(E)$ relative to the angle-averaged result $\overline{F}_{\theta_0,180^\circ}(E)$, because of the preferential tendency for photons to be emitted in the forward hemisphere (relative to the incoming electron velocity – Figure 7) and hence the smaller number of electrons needed. However, at very low values of $\theta_0 \lesssim 30^\circ$, the required $\overline{F}_{\theta_0,\alpha}(E)$ is, for low energies, *greater* than both the $\theta_0 = 45^\circ$ case and the angle-averaged case (dashed line); this is a consequence of the angular behavior of $q(\epsilon, E, \theta)$ (in particular the low value near $\theta = 0$) shown in Figure 7 and noted at the end of §2. The greatest deviations between the correct spectrum and that deduced using the angle-averaged cross section are thus achieved for $\theta_0 \simeq 45^\circ$ (correct spectrum steeper) and for $\theta_0 \simeq 180^\circ$ (correct spectrum flatter).

Figure 5 shows the variation of the local spectral index δ_E as a function of E, for the $\theta_0 = 130^\circ$ spectra of Figure 3. Compared to the results for the isotropic case ($\alpha = 180^\circ$), the spectral indices for the anisotropic electron distributions are substantially smaller (flatter spectrum) at low energies ($\sim 40 \lesssim 200$ keV), and larger (steeper spectrum) at high energies ($\gtrsim 200$ keV). In all cases the value of δ_E increases with decreasing energy below ~ 50 keV,

indicative of the transition to a softer, more thermal, spectrum. At low energies $\lesssim 25$ keV, the value of δ_E changes to a form that increases with E, indicative of the general steepening trend associated with thermal spectra.

6. Conclusions

In determining the mean source electron population $\overline{F}(E)$ responsible for a given hard X-ray spectrum, it is very important to use a bremsstrahlung cross-section Q that accurately represents the geometric relationship between the source and the observer. Although the correct range of viewing angles (relative to the incoming electron direction[s]) requires modeling of the electron transport beyond the scope of the present paper, we have shown through a parametric analysis that use of an angle-averaged cross-section can lead to significant differences in $\overline{F}(E)$, especially at electron energies $\gtrsim 50$ keV.

Different mean source electron spectra $\overline{F}(E)$ correspond to different requirements on the electron injection spectrum $F_0(E_0)$. Specifically, for collisional energy losses in a cold (but fully ionized) target, $F_0(E_0)$ is related to $\overline{F}(E)$ by (Brown & MacKinnon 1985; Emslie 2003)

$$F_0(E_0) = -\frac{K\,\overline{n}\,V}{A}\frac{d}{dE}\left[\frac{\overline{F}(E)}{E}\right], \tag{13}$$

where A is the injection area (cm^2) and $K = 2\pi e^4\Lambda$, e being the electronic charge and Λ the Coulomb logarithm. The injected power P^* (ergs s^{-1} above reference energy E^*) is therefore

$$P^* = A\int_{E^*}^{\infty} E_0\,F_0(E_0)\,dE_0 = K\overline{n}\,V\,\left[\overline{F}(E^*) + \int_{E^*}^{\infty}\frac{\overline{F}(E)}{E}\,dE\right], \tag{14}$$

where we have used integration by parts in the last equality. Figure 6 shows the variation of the P_{30} (i.e, P^* with $E^* = 30$ keV) required to produce the hard X-ray spectrum of Figure 2 as a function of the mean viewing angle θ_0 for various values of the cone half-angle α. In general, as θ_0 increases, the electrons become less efficient at radiating toward the observer (see Figure 7) and so the required P_{30} increases. However, as the spread in beam directions α increases, the value of P_{30} relaxes back to the angle-averaged value. This trend is reversed at very low ($\lesssim 30^\circ$) values of both θ_0 and α: the required power is slightly *greater* than for the angle-averaged cross-section. As discussed in §5, this is because at low energies, the cross-section peaks at an angle substantially different from zero (see Figure 7). As can be seen from the first panel in Figure 4, the mean source electron flux for $(\theta_0 = 0, \alpha = 0)$ is *greater*

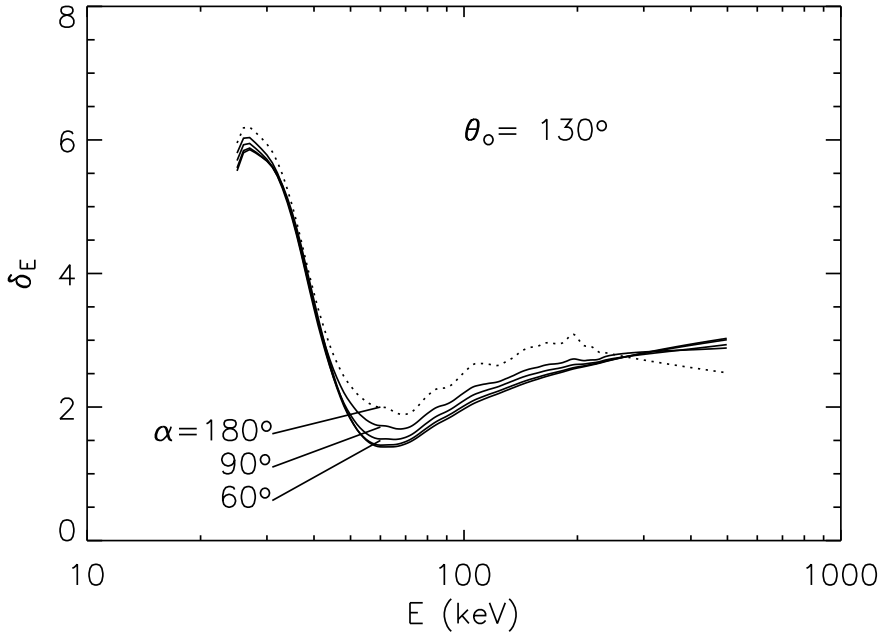

Fig. 5.— Spectral index variation for $\theta_o = 130°$ and values of α indicated.

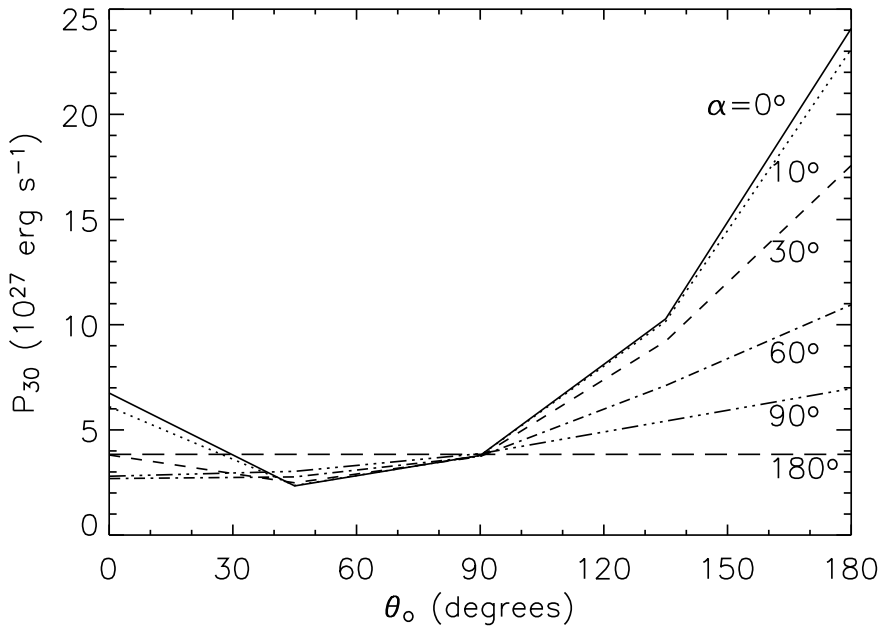

Fig. 6.— Injected power P_{30} as a function of θ_o for various values of α.

than the angle-averaged result for energies $E \lesssim 50$ keV, and electrons in the $(30 - 50)$ keV range dominate the contribution to the total injected power.

In summary, the use of the correct, direction-dependent cross-section can yield recovered mean source electron spectra of significantly different shape, and corresponding injected powers with a significantly different total injected energy, than the results using the usual angle-averaged (e.g., Haug 1997) cross-section. Recognizing that the total hard X-ray production also includes a contribution from the (angle-dependent) contribution from secondary (photospherically backscattered) photons (Tomblin 1972; Santangelo, Horstman, & Horstman-Moretti 1973; Langer & Petrosian 1977; Bai & Ramaty 1978), in future works we plan to incorporate an empirical treatment of this effect (e.g., Alexander & Brown 2002) as a correction to the angle-dependent cross-sections used.

This work was supported by NASA's Office of Space Science through Grant NAG5-207745, by a PPARC Grant, and by a collaboration grant from the Royal Society. We thank Dr. Gordon Holman for his critical review of the manuscript, which led to the sharpening of many of the ideas presented.

A. Form of the Angle-Dependent Bremsstrahlung Cross-Section

The cross-section $Q(\epsilon, E; \theta)$ used in this work has been presented by Gluckstern & Hull (1953) and Koch & Motz (1959). Here we reprint this result in our notation (and in units of cm^2 keV^{-1} sr^{-1}), and we also present a polar diagram of the angular dependence for various electron and photon energies, in order to make some of the discussions in the paper more comprehensible.

Formally, the cross-section $Q(\epsilon, E; \theta)$ for electron-ion bremsstrahlung, differential in photon energy ϵ, electron energy E, and the angle θ between the incoming electron and the emitted photon (but integrated over the direction of the emergent electron and summed over the polarization states of the emitted photon) is

$$
\begin{aligned}
Q(\epsilon, E; \theta) \quad &= \quad Z^2 \, \frac{\alpha}{2} \, \frac{r_0^2}{m_e c^2} \, \left(\frac{1}{\tilde{\epsilon}} \right) \frac{\sqrt{(\tilde{E} - \tilde{\epsilon})^2 - 1}}{\sqrt{\tilde{E}^2 - 1}} \; \times \\
&\times \quad \left\{ 8 \, \frac{2\tilde{E}^2 + 1}{(\tilde{E}^2 - 1)\Delta^4} \, \sin^2 \theta - 2 \, \frac{5\tilde{E}^2 + 2\tilde{E}(\tilde{E} - \tilde{\epsilon}) + 3}{(\tilde{E}^2 - 1)\Delta^2} \; - \right.
\end{aligned}
$$

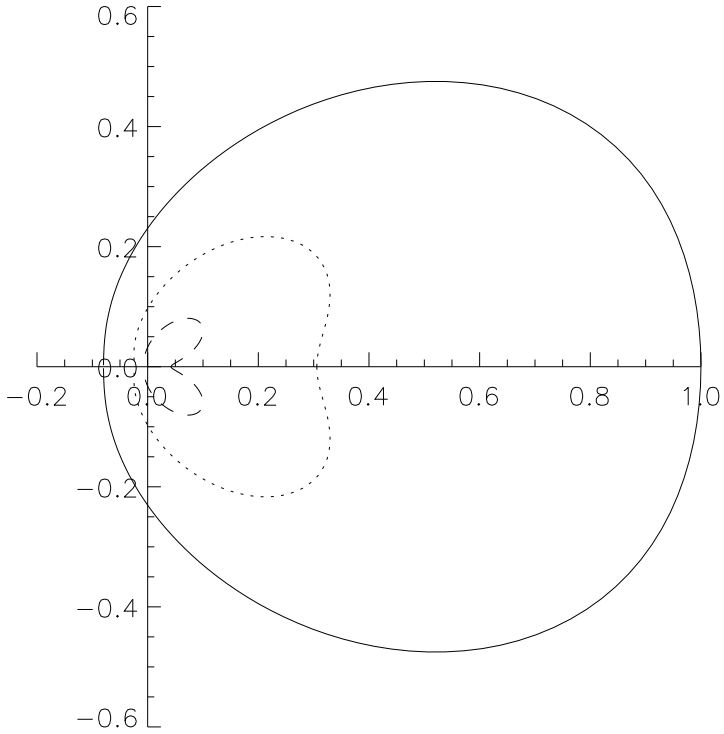

Fig. 7.— Polar diagram of the bremsstrahlung cross-section for $E = 100$ keV and photon energies $\epsilon = 30$ keV (solid line), $\epsilon = 50$ keV (dotted line), and $\epsilon = 80$ keV (dashed line); the radial coordinate is proportional to the size of the cross-section and the angle from the x-axis corresponds to the angle between the incoming electron direction and the line to the observer. Note that at energies $E \gg \epsilon$ the cross-section peaks at $\theta = 0$, while for $E \simeq \epsilon$ the cross-section peaks at $\theta \simeq (30 - 40)^\circ$.

$$
\begin{aligned}
&- \;\; 2\,\frac{\tilde{E}^2-\tilde{\epsilon}^2-1}{T^2\Delta^2} \;+\; 4\,\frac{\tilde{E}-\tilde{\epsilon}}{(\tilde{E}^2-1)\Delta} \;+ \\
&+ \;\; \frac{L}{\sqrt{([\tilde{E}-\tilde{\epsilon}]^2-1)(\tilde{E}^2-1)}}\Bigg[\frac{4\tilde{E}\,(3\tilde{\epsilon}-[\tilde{E}^2-1][\tilde{E}-\tilde{\epsilon}])}{(\tilde{E}^2-1)\,\Delta^4}\,\sin^2\theta + \\
&\quad + \;\; \frac{4\tilde{E}^2(\tilde{E}^2+[\tilde{E}-\tilde{\epsilon}]^2)-2(7\tilde{E}^2-3\tilde{E}[\tilde{E}-\tilde{\epsilon}]+[\tilde{E}-\tilde{\epsilon}]^2)+2}{(\tilde{E}^2-1)\Delta^2} + \\
&\quad + \;\; 2\,\tilde{\epsilon}\,\frac{\tilde{E}^2+\tilde{E}(\tilde{E}-\tilde{\epsilon})-1}{(\tilde{E}^2-1)\Delta}\Bigg] + \\
&+ \;\; \frac{\gamma_T}{T\,\sqrt{(\tilde{E}-\tilde{\epsilon})^2-1}}\Big[\frac{4}{\Delta^2}-\frac{6\tilde{\epsilon}}{\Delta}-\frac{2\tilde{\epsilon}\,(\tilde{E}^2-\tilde{\epsilon}^2-1)}{T^2\Delta}\Big] - \\
&- \;\; \frac{4\gamma}{\Delta\,\sqrt{(\tilde{E}-\tilde{\epsilon})^2-1}}\Bigg\}\times\frac{\beta(1-e^{-2\pi Z\alpha/\beta})}{\beta'(1-e^{-2\pi Z\alpha/\beta'})} \quad , \qquad \text{(A1)}
\end{aligned}
$$

where Z is the atomic number of the ion, $\alpha \simeq 1/137$ is the fine structure constant, $r_0 \simeq 2.8\times10^{-13}$ cm is the classical electron radius, $m_e c^2 \simeq 511$ keV is the electron rest energy, and

$$
\tilde{E} = 1+\frac{E}{m_e c^2}\,; \qquad \tilde{\epsilon} = \frac{\epsilon}{m_e c^2}\,; \qquad \beta = \sqrt{1-\frac{1}{\tilde{E}^2}}\,; \qquad \beta' = \sqrt{1-\frac{1}{(\tilde{E}-\tilde{\epsilon})^2}}, \qquad \text{(A2)}
$$

$$
\Delta = \tilde{E} - \sqrt{\tilde{E}^2-1}\,\cos\theta, \qquad \text{(A3)}
$$

$$
T = (\tilde{E}^2-1+\tilde{\epsilon}^2-2\tilde{\epsilon}\sqrt{\tilde{E}^2-1}\,\cos\theta)^{1/2}, \qquad \text{(A4)}
$$

$$
L = \ln\left[\frac{\tilde{E}(\tilde{E}-\tilde{\epsilon})-1+\sqrt{(\tilde{E}^2-1)([\tilde{E}-\tilde{\epsilon}]^2-1)}}{\tilde{E}(\tilde{E}-\tilde{\epsilon})-1-\sqrt{(\tilde{E}^2-1)([\tilde{E}-\tilde{\epsilon}]^2-1)}}\right], \qquad \text{(A5)}
$$

$$
\gamma_T = \ln\left[\frac{T+\sqrt{(\tilde{E}-\tilde{\epsilon})^2-1}}{T-\sqrt{(\tilde{E}-\tilde{\epsilon})^2-1}}\right], \qquad \text{(A6)}
$$

and

$$\gamma = \ln \left[\frac{(\tilde{E} - \tilde{\epsilon}) + \sqrt{(\tilde{E} - \tilde{\epsilon})^2 - 1}}{(\tilde{E} - \tilde{\epsilon}) - \sqrt{(\tilde{E} - \tilde{\epsilon})^2 - 1}} \right]. \tag{A7}$$

The last factor in Equation (A1) (involving the velocity β [in units of the speed of light c]) is the Elwert (1939) Coulomb correction and does not appear in the expressions in Gluckstern & Hull (1953). This correction is sufficiently accurate (to within a few percent) except at electron energies above ~ 100 keV and approaching the "high-frequency limit" $\epsilon \rightarrow E$; in such regimes more elaborate expressions are appropriate. For more details, see Koch & Motz (1959).

It should be noted that the expression (A1) is indeterminate at $\epsilon = E$; in practice this can be handled in numerical computation by setting E slightly higher than ϵ.

Figure 7 shows the angular dependency of the cross-section given by Equation (A1). The strong beaming of emission in direction of the incoming electron ($\theta = 0$) at high energies, and the peak near $\theta = 30^\circ$ at lower energies, are evident.

REFERENCES

Alexander, R.C., & Brown, J.C. 2002, Sol. Phys., 210, 407

Bai, T. & Ramaty, R. 1978, ApJ, 219, 705

Brown, J.C. 1971, Sol. Phys., 18, 489

Brown, J.C. 1972, Sol. Phys., 26, 441

Brown, J.C., & Emslie, A.G. 1988, ApJ, 331, 554

Brown, J.C., Emslie, A.G., & Kontar, E.P. 2003, ApJ, 595, L115

Brown, J.C. & MacKinnon, A.L. 1985, ApJ, 292, L31

Elwert, G. 1939, Ann. Physik, 34, 178

Elwert, G. & Haug E. 1970, Sol. Phys., 15, 234

Elwert, G. & Haug E. 1971; Sol. Phys., 20, 413

Emslie, A. G. 2003, ApJ, 595, L119

Emslie, A.G., Miller, J.A., & Brown, J.C. 2004, ApJ, 602, L69

Gluckstern, R.L., Hull, M.H., & Breit, G. 1953, Phys. Rev., 90, 1026

Gluckstern, R.L., & Hull, M.H. 1953, Phys. Rev., 90, 1030

Haug, E. 1972, Sol. Phys., 25, 425

Haug, E. 1997, A&A, 326,417

Hénoux, J.-C. 1975, Sol. Phys., 42, 219

Hurford, G.J., Schwartz, R.A., Krucker, S., Lin, R.P., Smith, D.M., & Vilmer, N. 2003, ApJ, 595, L77

Koch, H.W., & Motz J.W., 1959, Phys. Rev., 31, 920

Kontar, E.P., 2001, Solar Phys., 202, 131

Kontar, E.P., & Pecseli H.L., 2002, Phys. Rev. E, 65, 066408

Kontar, E.P., Piana, M., Massone, A.M., Emslie, A.G., & Brown, J.C. 2004, Sol. Phys., submitted

Langer, S. H., & Petrosian, V. 1977, ApJ, 215, 666

Leach, J., & Petrosian, V. 1981, ApJ, 251, 781

Leach, J., & Petrosian, V. 1983, ApJ, 269, 715

Piana, M., Massone, A. M., Kontar, E.P., Emslie, A.G., Brown, J.C., & Schwartz, R.A. 2003, ApJ, 595, L127

Santangelo, N., Horstman, H., & Horstman-Moretti, E. 1973, Sol. Phys., 29, 143

Smith, D.M., et al. 2002, Sol. Phys., 210, 33

Smith, D.M., Share, G.H., Murphy, R.J., Schwartz, R.A., Shih, A.Y., & Lin, R.P. 2003, ApJ, 595, L81

Stepanov, A.V., & Tsap, Y.T., Sol. Phys., 211, 135

Tomblin, F.F. 1972, ApJ, 171, 377